buildings

MDPI

Article

Identification and Diagnosis of Wind Health-Vulnerable Spaces in High-Rise Residential Areas of Xi'an

Jiewen Chen [1], Siqing Ma [1], Yuan Meng [1], Yu Liu [2] and Juan Ren [1,3,*]

[1] School of Architecture, Chang'an University, Xi'an 710061, China
[2] School of Mechanics, Civil Engineering and Architecture, Northwestern Polytechnical University, Xi'an 710072, China; liuyu@nwpu.edu.cn
[3] School of Architecture, Xi'an University of Architecture and Technology, Xi'an 710055, China
* Correspondence: juanren@chd.edu.cn; Tel.: +86-29-8233-7241

Abstract: As urbanization accelerates, high-rise residential areas (HRRAs) have become a dominant urban housing typology. However, their complex building layouts significantly alter local wind environments, potentially impacting residents' health. While existing studies mainly focus on macro-scale wind analysis, there is limited exploration of the micro-environmental interactions between wind conditions and human activities. This study proposes the concept of Wind Health-Vulnerable Space (WHVS) and addresses the following scientific question: How do building layouts affect local wind fields and influence pollutant accumulation and health risks, particularly for air pollutants like PM2.5 (particulate matter with an aerodynamic diameter of 2.5 μm or less), which is closely associated with adverse respiratory and cardiovascular health outcomes? To investigate this, a multidimensional framework integrating computational fluid dynamics (CFD) simulations with point-of-interest (POI) data was developed to identify and diagnose these spaces. Case studies of two typical HRRAs in Xi'an, China, reveal two types of WHVSs: (1) localized calm zones between buildings (wind speed < 0.5 m/s, pressure −0.5 to 3 Pa), where PM2.5 concentrations are 25–30% higher than surrounding areas; and (2) large-scale weak wind areas in enclosed layouts (wind speed < 0.5 m/s, pressure −1 to −2 Pa), with PM2.5 concentrations increased by 28–35%. The results highlight a dual mechanism in the formation of vulnerable spaces: wind field disturbances caused by building layout and the overlay effect of human activity distribution. This framework offers new insights and scientific support for health-oriented urban planning and building layout optimization.

Keywords: wind health-vulnerable spaces; high-rise residential areas; computational fluid dynamics; point-of-interest data fusion; PM2.5

Academic Editor: David J. Edwards

Received: 25 March 2025
Revised: 28 April 2025
Accepted: 30 April 2025
Published: 2 May 2025

Citation: Chen, J.; Ma, S.; Meng, Y.; Liu, Y.; Ren, J. Identification and Diagnosis of Wind Health-Vulnerable Spaces in High-Rise Residential Areas of Xi'an. *Buildings* **2025**, *15*, 1538. https://doi.org/10.3390/buildings15091538

1. Introduction

1.1. Background and Literature Review

With the acceleration of global urbanization, high-rise residential areas (HRRAs) have become the primary solution to address urban housing demands. According to the United Nations Human Settlements Programme, by 2050, the global urban population is projected to reach 68%, with Asia experiencing the fastest rate of urbanization [1]. This trend is particularly pronounced in China, where the development of HRRAs has emerged as a dominant strategy to mitigate land resource scarcity and rising population density. Some studies suggest that high-rise buildings constitute a substantial proportion—reportedly over 65%—of urban residential structures in China [2].

Urban residential areas merit particular attention because they are where people spend the majority of their time, with residents typically experiencing 12–16 h of daily exposure to local environmental conditions [3]. This extended exposure period amplifies the health implications of any environmental quality issues in these spaces.

The complex interactions between building forms and local meteorological conditions significantly impact the environmental health of HRRAs. Recent studies have shown that the dense layout of high-rise buildings alters local wind field characteristics in two primary ways: first, by creating calm zones with wind speeds below 0.5 m/s between buildings [4–6]; and second, by forming high-wind corridors that can exceed 5 m/s [7]. These wind field modifications directly influence the dispersion and accumulation of air pollutants, particularly fine particulate matter (PM2.5).

PM2.5 (particulate matter with an aerodynamic diameter less than 2.5 μm) is a critical air pollutant that poses significant health risks due to its ability to penetrate deep into the respiratory system and enter the bloodstream. Numerous epidemiological studies have linked PM2.5 exposure to increased morbidity and mortality from respiratory and cardiovascular diseases [8,9]. In China, where PM2.5 concentrations frequently exceed the WHO guidelines, especially during winter, this pollutant represents a major public health concern in urban areas [10].

Previous research on wind environments in urban contexts has primarily focused on three distinct approaches. Macro-scale studies [11,12] have examined city-wide air movement patterns but lack resolution at the neighborhood level. Building-specific investigations [13,14] have analyzed wind dynamics around individual structures without considering the complex interactions in residential clusters. Ventilation-centered research [15,16] has emphasized airflow rates without directly connecting to health outcomes. Recent studies have further revealed that certain high-rise layouts, such as podium-connected tower clusters, significantly reduce pollutant dispersion efficiency under stable winter conditions [17]. A comprehensive comparison of relevant studies in the field of urban wind environment and health impacts is provided in Appendix A, which highlights the methodological approaches, key findings, and limitations of existing research. Meanwhile, a recent study has proposed a Wind Health Risk Index (WHRI) by integrating CFD, GIS, and health risk assessment, offering a novel framework for urban environmental health evaluation [18].

Xi'an, located in Northwestern China, represents an ideal case study for several reasons. First, the city experiences severe PM2.5 pollution during winter months, with concentrations regularly exceeding 150 $\mu g/m^3$, significantly higher than the WHO guideline of 5 $\mu g/m^3$ for 24 h exposure [19]. Second, Xi'an has undergone rapid high-rise residential development, with over 70% of new housing constructed as high-rise buildings in the past decade [20]. Third, its semi-arid climate with distinct seasonal variations provides an opportunity to study wind–pollutant interactions under challenging meteorological conditions that exacerbate pollution accumulation [21].

1.2. Research Gap and Significance

Despite the extensive body of research on urban wind environments and air pollution, there remains a critical gap in understanding the micro-environmental interactions among wind conditions, pollutant dispersion, and human activity patterns at the residential cluster level. This gap is characterized by several limitations in existing approaches.

1. Scale discontinuity: Most studies either focus on macro-scale atmospheric processes [22,23] or highly localized building aerodynamics [24], missing the critical meso-scale where residents experience their environment.

2. Disciplinary isolation: Environmental engineering research rarely incorporates human behavioral data [25], while public health studies often use generalized exposure estimates without spatial specificity [26].
3. Methodological limitations: Studies typically rely on either computational models or field measurements in isolation, rather than validating simulations with empirical data [27].
4. Disconnected applications: Design recommendations often emerge from isolated performance metrics rather than integrated health-centered evaluations [28,29].

This study addresses these limitations by introducing the concept of Wind Health-Vulnerable Space (WHVS), defined as areas where adverse wind conditions (low ventilation or high turbulence) intersect with zones of intensive human activity, resulting in elevated exposure to air pollutants, particularly PM2.5.

1.3. Theoretical Framework

WHVS is defined as specific areas within HRRAs where adverse wind conditions (e.g., stagnant airflow, pollutant accumulation) spatially coincide with high-frequency human activities, leading to elevated health risks. This concept integrates three critical dimensions, shown in Figure 1.

1. Wind environment dynamics (low wind speed, turbulence, abnormal pressure).
2. Pollutant dispersion (localized pollution due to poor airflow).
3. Human activity exposure (spatial coincidence of dense activity with pollutant-prone zones).

The WHVS framework is grounded in four interrelated attributes: physical interactivity links wind field anomalies such as vortex formation with pollutant dispersion efficiency; exposure–sensitivity coupling indicates that dense human activity within poorly ventilated zones significantly elevates health risks; temporal dynamics captures how diurnal and seasonal variations in wind and activity patterns influence exposure levels, as seen in winter stagnation periods; and scale dependency highlights the need to assess micro-scale interactions at the building cluster level rather than relying on generalized city-wide metrics. This framework bridges spatial vulnerability theory and CFD-based urban aerodynamics, addressing the disconnect between environmental modeling and socio-behavioral realities. By framing WHVS as a coupled socio-physical system, the study advances health-oriented urban design from fragmented symptom management to integrated mechanism diagnosis.

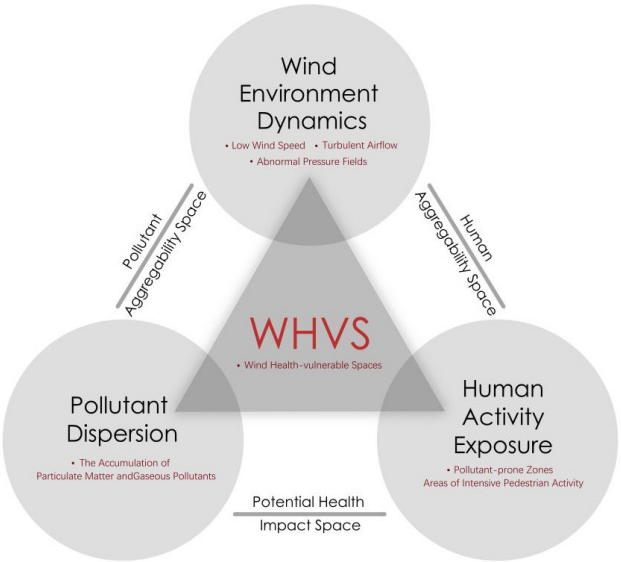

Figure 1. Conceptual definition of WHVS.

To support the WHVS framework both conceptually and methodologically, this study incorporates three foundational theories. These theories are further elaborated below and summarized in Table 1.

1. Spatial Vulnerability Theory

Originally proposed by Turner et al. [30], this theory conceptualizes vulnerability as a system's sensitivity to external stressors and its adaptive capacity. Here, the system refers to the micro-environment of HRRAs, comprising (i) wind environments shaped by building layouts, (ii) pollutant dispersion processes, and (iii) human activity patterns. External stressors include both physical disturbances (e.g., wind field distortion from dense buildings) and socio-behavioral pressures (e.g., activity clustering in stagnant zones). Building on Turner's triad of exposure, sensitivity, and adaptive capacity, this study constructs a diagnostic WHVS framework: exposure is mapped via CFD-simulated wind speed and pressure fields; sensitivity is derived from POI-based population activity densities; and adaptive capacity is evaluated through potential building layout improvements that enhance ventilation and reduce risk. This integration bridges physical environmental modeling and socio-spatial behaviors, enabling a comprehensive diagnosis of WHVS formation mechanisms.

2. Building Environmental Dynamics

This theory underpins the interaction between built form and local airflow. Drawing on Blocken et al. [31], the study focuses on airflow characteristics in high-rise clusters, including flow separation, vortex formation, and negative pressure zones—all of which influence pollutant retention. Specifically, we analyze wind speed and pressure distribution patterns under different layout conditions to understand how building form contributes to the emergence of low-ventilation, high-risk zones.

3. Environmental Health Exposure Theory

This framework explains how environmental risks translate into health impacts through exposure mechanisms [20]. We adopt three key components: (1) POI-based hotspot analysis to identify high-activity zones; (2) spatial coupling of human activity with poor wind environments to detect health risk convergence areas; and (3) PM2.5 field monitoring to empirically validate CFD simulations and support WHVS identification.

The integration of these three theoretical frameworks forms the theoretical foundation of this study: the spatial vulnerability theory provides the overall analytical framework, the building environment dynamics theory guides the simulation and analysis of the wind environment, and the environmental health exposure theory supports the identification of population exposure characteristics. Through the methodical synthesis of these complementary perspectives, a WHVS identification and diagnostic method suitable for building-scale applications wass developed, providing theoretical support for optimizing the healthy environment of HRRA.

Table 1. Logical relationships among the three theoretical frameworks.

Theoretical Framework	Core Focus	Role in WHVS	Logical Relationship with Other Theories
Spatial Vulnerability Theory	Susceptibility of spatial units to risks based on population, environment, and structure	Basis for identifying vulnerable spaces via exposure, sensitivity, and adaptability	Provides socio-spatial context for exposure; combines with dynamics to locate environmental risk zones

Table 1. *Cont.*

Theoretical Framework	Core Focus	Role in WHVS	Logical Relationship with Other Theories
Built Environment Dynamics Theory	Impact of urban form on airflow, heat, and pollutant dispersion	Explains spatial mechanisms of WHVS through CFD simulation	Defines physical exposure patterns; complements vulnerability theory to locate risk-prone areas
Environmental Health Exposure Theory	Exposure level and duration in space and time	Links wind and pollution exposure to potential health effects	Adds health risk dimension by overlaying exposure onto socially and physically vulnerable spaces

1.4. Research Objectives

This study aims to carry out the following:

1. Develop and validate a multidimensional framework for identifying WHVSs in high-rise residential areas.
2. Analyze the formation mechanisms of Wind Health-Vulnerable Spaces in two contrasting urban layouts.
3. Establish evidence-based recommendations for health-oriented urban planning and building layout optimization.

The subsequent sections detail the methodological approach and present findings that advance health-oriented urban design from fragmented symptom management to integrated mechanism diagnosis, offering new insights for optimizing building layouts to reduce health risks in high-density urban environments.

2. Materials and Methods

2.1. Research Framework

This study employs a multidimensional framework for identifying and diagnosing Wind Health-Vulnerable Spaces (WHVSs) in high-rise residential areas, integrating wind environment analysis, pollutant dispersion modeling, and human activity pattern assessment. The research process consists of five key components.

(1) Geometric Modeling: Constructing 3D building models of the study areas using ArcGIS 10.8 software to prepare for wind environment simulation and spatial analysis.
(2) Wind Environment Simulation: Conducting computational fluid dynamics (CFD) simulations to analyze wind speed, wind pressure, and pollutant dispersion characteristics.
(3) Spatial Analysis: Using POI data to identify human activity hotspots and assess their spatial overlap with adverse wind environments.
(4) Field Monitoring: Measuring PM2.5 concentrations at multiple monitoring points to validate the simulation results and assess air quality conditions.
(5) Integrated Assessment: Combining wind environment characteristics, pollutant dispersion patterns, and human activity data to identify and diagnose WHVSs.

The research framework is illustrated in Figure 2.

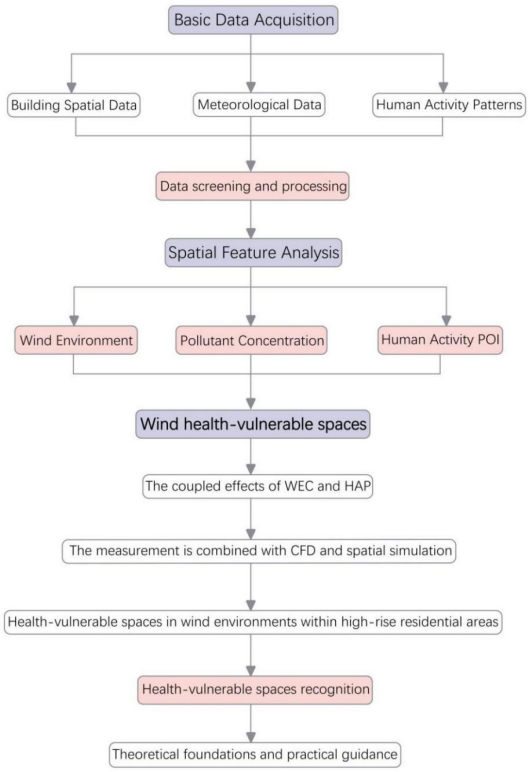

Figure 2. Research framework for WHVS.

2.2. Data Collection and Processing

The data collection and processing phase involved gathering and preparing multiple types of data to support the numerical simulations and spatial analyses. The following data were collected and processed:

First, building spatial data for CASE A and CASE B, including layouts, density, and height, were collected to construct 3D building models (Figure 3). Topographic data of Xi'an, covering buildings, road networks, and public spaces, were also obtained to support spatial analysis. The selected cases represent two common high-rise residential typologies in Chinese cities: CASE B features a high-density (FAR = 6.93), linear "row-type" layout, while CASE A reflects a medium-density (FAR = 2.63), enclosed "courtyard-type" configuration. The selection was based on their planning representativeness, coverage of typical FAR ranges (from mid- to super-high density), and observed PM2.5 accumulation during winter. CASE A's compact blocks generate localized low wind zones, while CASE B's enclosed form creates a broader weak-wind region, both contributing to pollution retention and health-related wind vulnerability under adverse climatic conditions.

In addition, meteorological data for Xi'an, including wind direction, wind speed, and temperature, were collected to configure the boundary conditions for the CFD simulations. The data primarily reflected natural conditions during the winter season, which is the primary research period due to the pronounced seasonal climatic characteristics of Xi'an and increased susceptibility to pollution accumulation.

To support human activity analysis, POI data from the two cases were collected, including information such as residential area names, building heights, and functional types. The data were cleaned and classified to facilitate spatial analysis. The data were cleaned and classified to facilitate spatial analysis. The raw POI data used in this study are publicly available and can be downloaded from: https://lbs.amap.com (see Supplementary Materials). Kernel density analysis and buffer analysis were employed to identify hotspots of human activity and evaluate human aggregation patterns within various distance ranges.

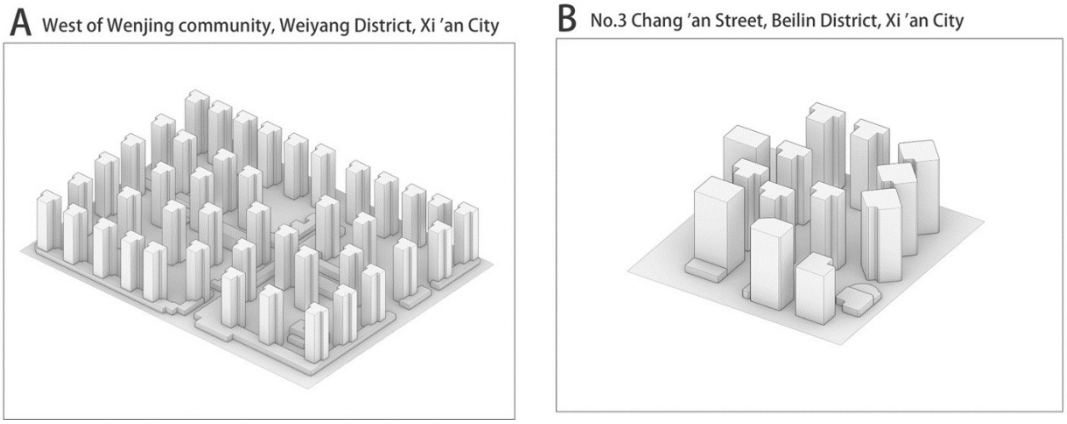

(**a**) (**b**)

Figure 3. Building mass models of two cases. (**a**) Geometric model of CASE A; (**b**) geometric model of CASE B.

Finally, on-site monitoring of PM2.5 concentrations was conducted during the winter season to capture variations in air quality across different time periods. Multiple monitoring points were established for CASE A and CASE B, covering key areas such as building clusters, courtyards, and main pedestrian pathways. The collected PM2.5 data underwent cleaning and preprocessing to remove outliers and noise, ensuring the reliability of the dataset for subsequent analysis.

2.3. Numerical Simulation of Wind Environment

The numerical simulation of the wind environment was conducted using CFD techniques to analyze wind speed, wind pressure, and pollutant dispersion characteristics in the study areas. All CFD simulations were conducted using ENVI-met 5.6.1, developed by ENVI-met GmbH, based in Essen, Germany, for flow field modeling and pollutant dispersion analysis. The 3D building model was constructed in Rhino 7.0 and meshed using Butterfly. GIS analysis and POI data processing were carried out in ArcGIS 10.8 with its Spatial Analyst extension. This section describes the key steps and parameter settings of the CFD simulation, as well as the validation of the simulation model.

2.3.1. CFD Parameter Settings and Boundary Conditions

The numerical simulation of the wind environment was conducted using CFD techniques, which offer several advantages over alternative methods for this study [27,32].

1. Spatial resolution: Unlike wind tunnel tests, CFD provides comprehensive data for every point in the computational domain, allowing for detailed analysis of complex flow patterns between buildings [5].
2. Cost efficiency: CFD simulations are more economical for parametric studies comparing multiple urban configurations.
3. Visualization capabilities: Advanced 3D visualization of flow fields enables better identification of problematic areas.
4. Integration potential: CFD results can be directly coupled with pollutant dispersion models and spatial analysis tools.

A high-precision three-dimensional building model was constructed based on the collected architectural spatial data. An unstructured mesh was employed for grid discretization, consisting of approximately 3.5 million cells with a minimum grid size of 0.2 m, ensuring computational accuracy within the simulation domain. The k-ε turbulence model

was selected due to its suitability for high Reynolds number flows and its ability to capture the flow characteristics around buildings effectively [33].

Boundary conditions were defined based on meteorological data from Xi'an, primarily reflecting natural conditions during winter. The inlet boundary conditions followed an exponential wind profile.

$$U(z) = U_r \left(\frac{z}{z_r} \right)^{\alpha}, \quad (1)$$

U(z) is the wind speed at high z. U_r is the wind speed at a reference height z_r (often taken as the wind speed near the ground or a known height). z is the height being considered. z_r is the surface roughness length (usually related to the surface characteristics). α is the wind speed gradient exponent, typically ranging from 0.1 to 0.4, with the exact value depending on the surface characteristics and atmospheric stability.

2.3.2. Verification

The simulation model was verified using wind tunnel experimental data from the Architectural Institute of Japan (AIJ) guidelines, as proposed by Tominaga et al. [34]. The dimensions of the central building in the model are 25 m × 25 m × 100 m, while the surrounding buildings are prototypically sized at 40 m × 40 m × 10 m, as shown in Figure 4. Wind speed measurements were carried out using an improved Irwin-type anemometer, with the probe installed at a height of 5 mm, representing a full-scale height of 1.5 m [35].

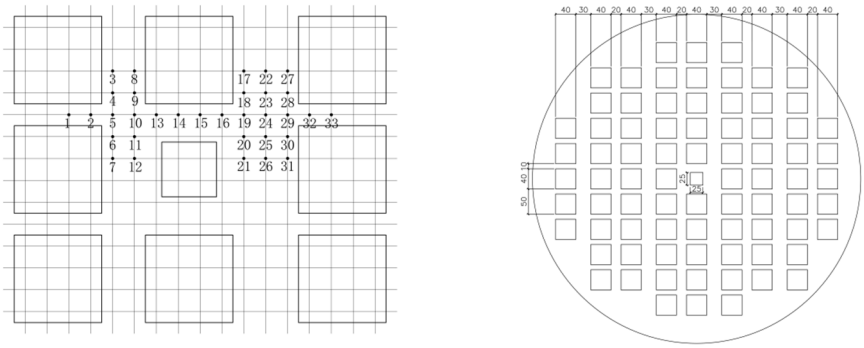

(**a**) (**b**)

Figure 4. Detailed diagram of pedestrian wind environment wind tunnel test. (**a**) Layout of measurement points for pedestrian wind environment. (**b**) Plan view of building model used in wind tunnel test for pedestrian wind environment.

The dimensionless wind speed ratio, RR, was used to compare the results of the wind tunnel experiments and CFD simulations. The wind speed ratio, RR, is defined as the ratio of the wind speed at a measurement point to the reference wind speed. The comparison between wind tunnel experiments and CFD simulations under an incoming wind direction angle of 0° is shown in Figure 5.

The results indicate that the wind speed ratio (RR) values at various measurement points exhibit consistent trends between wind tunnel experiments and CFD simulations, as shown in Figure 6. By analyzing three metrics—root mean square error (RMSE), mean absolute percentage error (MAPE), and coefficient of determination (R^2)—the average error of the wind speed ratio was calculated to be approximately 11.83%. A further investigation into the error sources revealed three primary contributors: CFD simulation errors, inherent errors in wind tunnel experiments, and complex turbulence effects near the surface [35,36]. The comparison demonstrates a strong correlation between CFD simulations and the

experimental results, confirming the reliability of the simulation methods employed in this study [32].

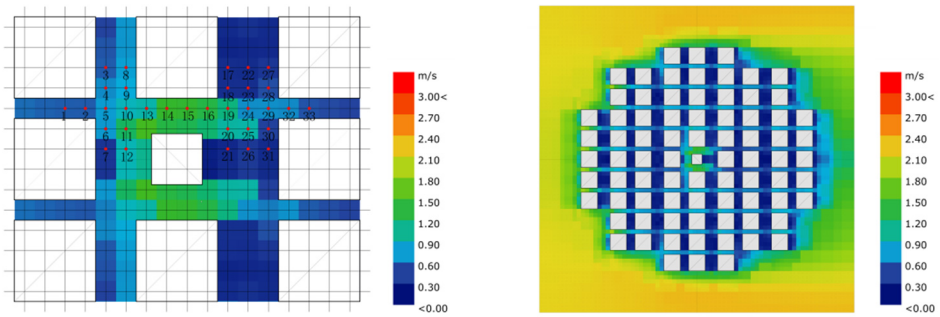

Figure 5. Detailed diagram of wind environment testing for standard model. (**a**) Wind speed contour map of test points; (**b**) vector wind environment contour map of standard model under 0° approaching wind direction.

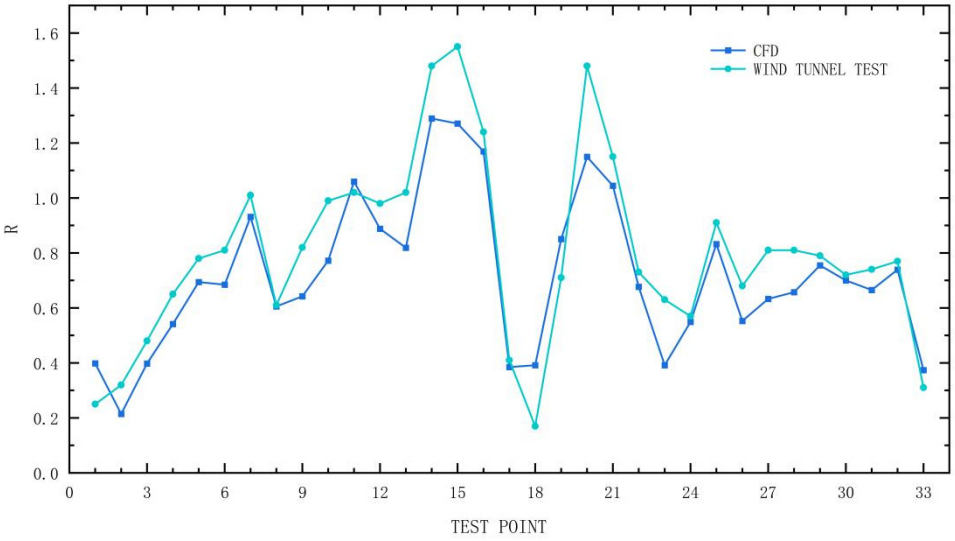

Figure 6. Comparison of simulation results with standard model data.

2.4. Field Monitoring Method

The monitoring device used was the AirNow air quality monitor, which employs laser detection for PM2.5, with a resolution of 1 μg/m^3 and a measurement range of 0–999 μg/m^3. The monitoring data covered the variation in PM2.5 concentration over different time periods, with measurements taken at 1 h intervals. Multiple monitoring points were established for CASE A and CASE B, covering key areas such as building clusters, courtyards, and main pedestrian pathways.

The monitoring period focused on the winter season, when adverse meteorological conditions and complex airflow patterns are most likely to lead to pollutant accumulation. Winter was selected as it represents the worst-case scenario for PM2.5 exposure in Xi'an, and prior studies [37] have shown that wind–pollution correlations peak during this season, facilitating clearer identification of Wind Health-Vulnerability Spaces (WHVSs). To ensure comprehensive spatial and temporal coverage, the monitoring points were strategically located to capture variations in air quality, as shown in Figure 7. The collected PM2.5 data underwent cleaning and preprocessing to remove outliers and noise, ensuring the reliability of the dataset for subsequent analysis.

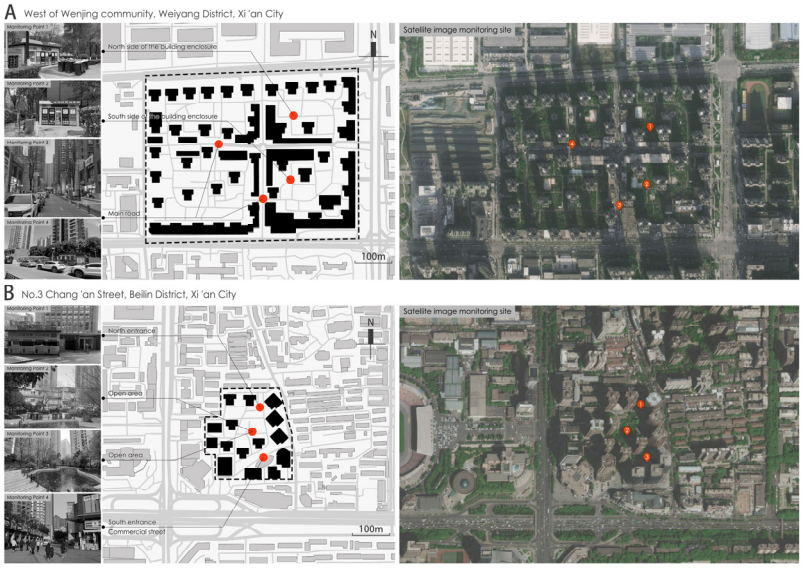

Figure 7. Measurement locations and corresponding sceneries for PM2.5 in two cases.

Based on the cleaned dataset, a time-series analysis approach was employed to perform statistical and trend analyses of PM2.5 concentrations at various monitoring points. The collected data were then compared with the CFD simulation results to investigate the impact of wind environment characteristics on air quality. Furthermore, the spatial distribution of PM2.5 concentrations was analyzed to identify areas with elevated pollution levels and their correlation with low wind speed zones.

2.5. Integrated Assessment Approach

To identify WHVSs effectively, this study developed an integrated assessment approach that combines the following:

1. Wind field analysis: Characterizing areas with wind speeds below 0.5 m/s and adverse pressure conditions.
2. Human exposure assessment: Overlaying activity density data with environmental risk factors.
3. Pollution potential mapping: Identifying zones where PM2.5 accumulation is likely based on CFD simulations and field measurements.

The integration of these three components enables the classification of urban spaces into severity categories based on combined risk factors, providing a more comprehensive understanding of health vulnerability than single-factor assessments. This approach bridges the gap between traditional aerodynamic studies and public health assessments, offering a more nuanced perspective on urban environmental health [32].

3. Results

3.1. Characteristics of Wind Environment

This section provides a detailed analysis of the WECs in two typical cases (CASE A and CASE B). Based on the CFD simulation results, combined with field monitoring data, the distribution patterns of the wind speed and wind pressure in each residential area are described. Furthermore, the underlying mechanisms and environmental impacts of these characteristics are explored.

1. CASE A: West of Wenjing Community

As shown in Figure 8, a continuous low pedestrian-level wind speed zone is observed between the building clusters on the northwest side of CASE A, with pedestrian-level wind

speed (PLWS) below 0.5 m/s, represented by a deep blue color. The PLWS distribution in this area indicates that the dense arrangement and relative positioning of the buildings result in the formation of a low-speed airflow zone among the building clusters. Such low PLWS zones are primarily concentrated in the gaps between buildings, where PLWS are significantly reduced, adversely affecting the overall ventilation efficiency.

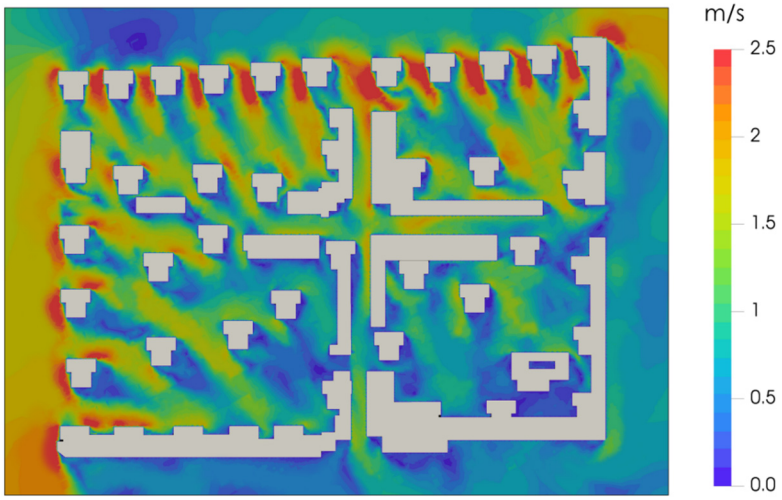

Figure 8. Wind speed distribution map of CASE A.

As illustrated in Figure 9, the wind pressure simulation map reveals that the low PLWS zone on the northwest side of CASE A is associated with relatively high pressure, with values ranging from approximately −0.5 to 3 Pa. The wind pressure distribution around the buildings exhibits significant variations, with negative pressure zones primarily concentrated in the shadowed areas of the buildings, reflecting the blocking and guiding effects of the structures on the incoming wind. This pattern of wind pressure distribution indicates that the building layout significantly influences the regional wind field, resulting in abnormal wind pressure in certain areas, which subsequently impacts ventilation and air quality.

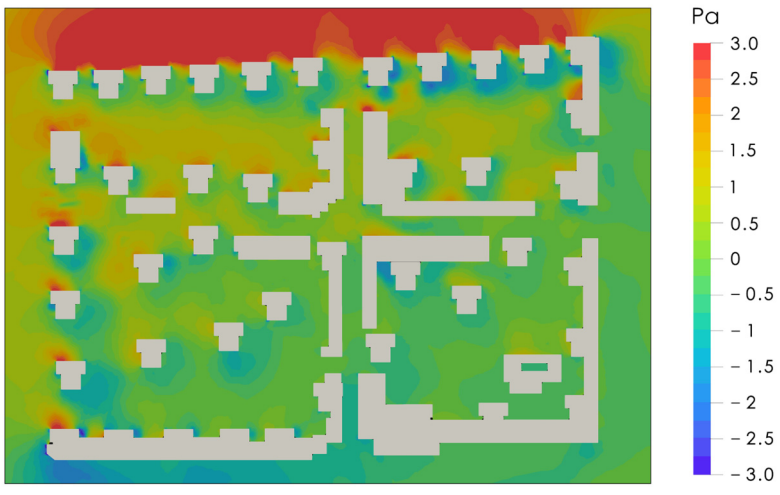

Figure 9. Wind pressure distribution map of CASE A.

The low wind speed zone between the building clusters on the northwest side and the semi-enclosed space formed by the central building clusters are the main wind environment features of CASE A. These areas, due to the dense building layouts, result in airflow dead zones and low-speed flow, which limit ventilation efficiency and affect air quality. The formation of these zones is primarily driven by the following mechanisms:

Flow Separation: The dense arrangement of buildings causes the incoming wind to separate, forming localized vortices and calm zones.

Pressure Anomalies: The blocking effect of the buildings creates negative pressure zones on the leeward side, further hindering pollutant dispersion.

2. CASE B: No. 3 Chang'an Street

As shown in Figure 10, according to the PLWS simulation map, a large low PLWS zone is observed on the southeast side of CASE B, with PLWSs consistently below 0.5 m/s, indicated by a deep blue color in the visualization. The PLWS distribution demonstrates a significant reduction in wind velocity, primarily concentrated on the leeward side of the building cluster and within the internal courtyard areas. This pattern reflects the strong blocking effect of the building cluster on the incoming wind flow.

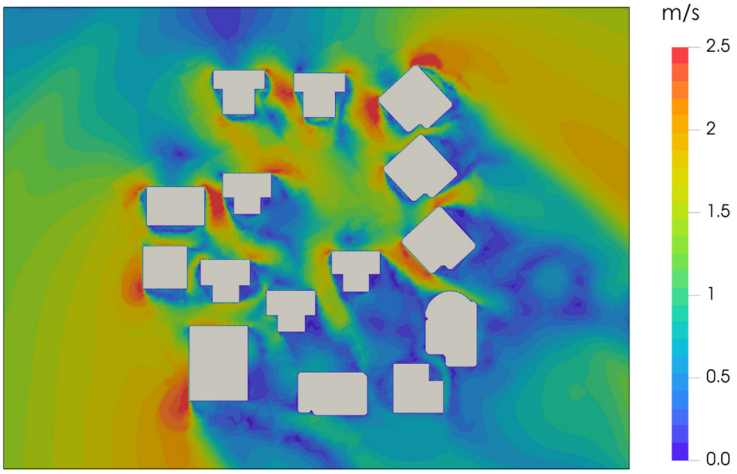

Figure 10. Wind speed distribution map of CASE B.

The wind pressure simulation reveals a notable negative pressure zone within the low wind speed region on the southeast side of CASE B, with pressure values ranging from approximately −1 to −2 Pa. Figure 11 provides a clear visualization of this phenomenon, where the negative pressure zones are concentrated primarily on the leeward side of the building cluster. This distribution highlights the pronounced influence of the structures on the wind field, causing large-scale separation zones to form on the leeward side. The wind pressure characteristics depicted in Figure 11 underscore how the overall layout of the building cluster significantly shapes the regional wind field, resulting in localized abnormal wind pressures that impact ventilation and air quality.

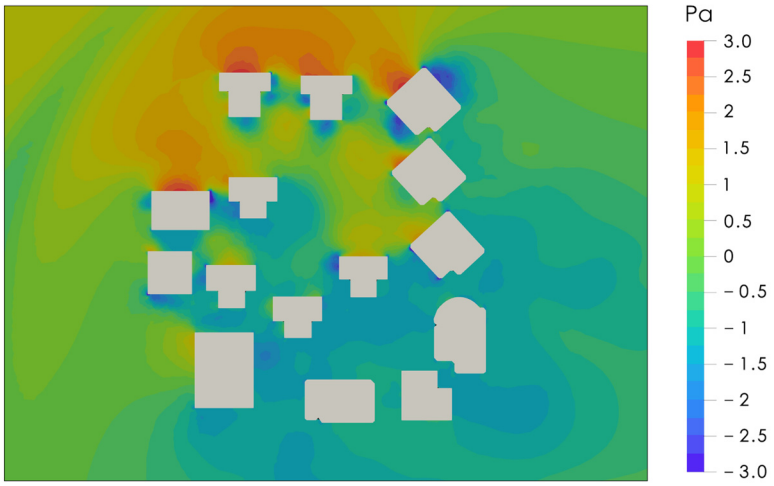

Figure 11. Wind pressure distribution map of CASE B.

The large low wind speed zone on the southeast side and the internal courtyard space are the main wind environment features of CASE B. Due to the overall blocking effect of the building clusters and the enclosure by high-rise buildings, large-scale airflow separation and stagnation occur, which restrict ventilation conditions and affect air quality. The formation of these zones is primarily driven by the following mechanisms:

Wind Shadow Effect: The high-rise buildings create a wind shadow on the leeward side, resulting in low wind speeds and poor ventilation.

Recirculation Patterns: The enclosed layout of the buildings promotes recirculation of airflow within the courtyard, leading to pollutant accumulation.

Wind speed and pressure simulations were used to characterize the wind environment and underlying mechanisms in CASE A and CASE B. The main distinctions are as follows: (1) Low Wind Speed Zones: CASE A exhibited localized calm areas (PLWS < 0.5 m/s) between northwest-facing buildings, whereas CASE B showed extensive weak wind zones on the southeast leeward side and within internal courtyards. (2) Wind Pressure Patterns: CASE A presented mild negative pressure (−0.5 to 3 Pa) in building wake zones, while CASE B showed stronger negative pressure (−1 to −2 Pa) in leeward areas. (3) Formation Mechanisms: Airflow separation and vortex formation in CASE A resulted from dense building configurations, whereas wind shadows and recirculation in CASE B were induced by its enclosed layout. (4) Impacts on Air Quality: Both cases revealed ventilation deficiencies, with localized pollutant buildup in CASE A and courtyard-scale stagnation in CASE B. These results indicate that compact and enclosed urban morphologies can significantly hinder airflow, contributing to the formation of Wind Health-Vulnerable Spaces (WHVSs).

3.2. Characteristics of Human Activities

This section analyzes human activity characteristics in two typical cases (CASE A and CASE B) using urban heat maps, identifying activity hotspots and their spatial distribution. These findings provide a basis for identifying WHVSs.

1. CASE A: West of Wenjing Community

The heat map of CASE A, as illustrated in Figure 12, indicates that human activities are predominantly concentrated at the core street intersections, with a clear high-activity density (indicated by the red areas). This phenomenon suggests that the core intersection, as the main transportation hub and a location concentrated with public service facilities, attracts a large number of residents and visitors, forming a significant gathering point for pedestrian flow. The surrounding areas, on the other hand, display lower activity densities (indicated by the blue areas), indicating that human activities are relatively dispersed, with a concentration primarily around residential buildings and green spaces.

High-activity density areas are clustered around public facilities (e.g., community squares, commercial streets), attracting residents and visitors with high frequency and long durations. In contrast, residential and green spaces show lower activity density, with shorter and more dispersed activities.

The core intersection has significantly higher pedestrian flow and dwell time, indicating greater exposure to air quality risks. These high-intensity areas are critical for identifying WHVSs and require attention to ventilation and air quality.

2. CASE B: No. 3 Chang'an Street

As depicted in Figure 13, the heat map of CASE B illustrates the spatial distribution of activity density within the area. Similarly to CASE A, pedestrian activities in CASE B are concentrated around the main streets and buildings, forming clear high-activity density zones (red areas). However, compared to CASE A, the high-activity areas in CASE B are

more evenly distributed, with red zones extending not only to street intersections but also to nearby major commercial facilities and public spaces.

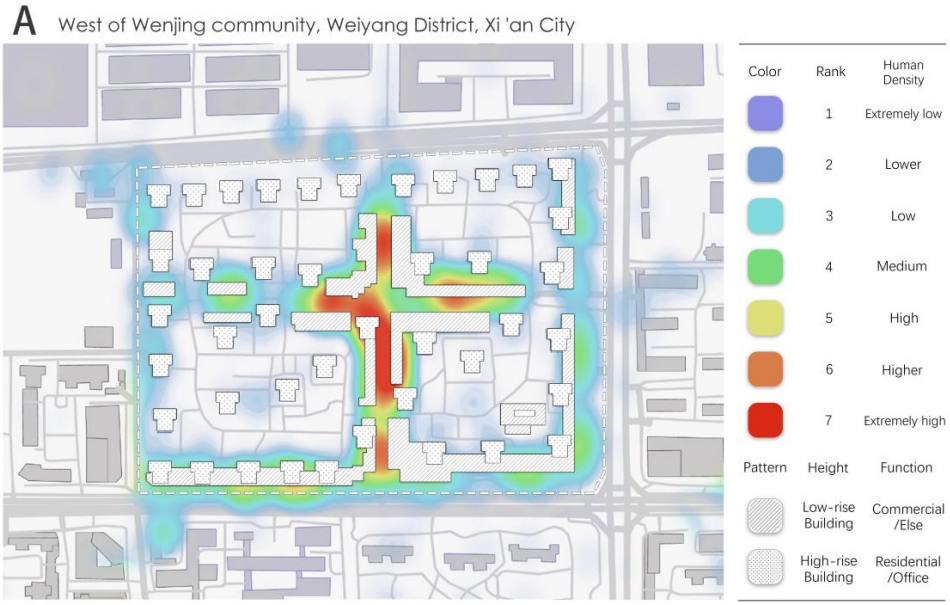

Figure 12. POI activity heat map of CASE A.

Figure 13. POI activity heat map of CASE B.

Activity is evenly distributed, with high-density zones around commercial, dining, and leisure areas. Residential areas also show moderate activity density, particularly in public corridors and near green spaces.

High-density areas experience significant pedestrian traffic and extended dwell times, especially around commercial and public service facilities. These zones are critical for air quality management due to their widespread distribution.

Both cases show human activity concentrated around major streets and public facilities, forming distinct hotspots. However, CASE A's hotspots are more focused on core intersections, while CASE B's are evenly distributed across multiple areas. High-activity density zones, due to human aggregation, are more vulnerable to air quality degradation,

highlighting the need to integrate wind environment characteristics and human activity patterns for accurate WHVS identification.

3.3. Identification of WHVS in Cases

Based on the results of outdoor wind environment simulation and human activity characteristics analysis, this section identifies the WHVSs in two typical cases. By integrating multidimensional indicators such as wind speed, wind pressure, population density, and activity intensity, the distribution characteristics and formation mechanisms of WHVS within each residential area are determined.

1. CASE A: West of Wenjing Community

In the northwest section of the residential building complex in CASE A, a contiguous area with wind speeds below 0.5 m/s was identified, as shown in Figure 14a. This area also exhibits a stable negative pressure zone, with pressure values ranging from approximately −0.5 to −1 Pa. The formation mechanism of this phenomenon is primarily attributed to the dense arrangement of buildings, which creates airflow stagnation zones within the complex and significantly reduces ventilation efficiency. Due to the consistently low wind speeds, air circulation in this region is severely restricted, facilitating the accumulation of pollutants. While the affected area remains relatively localized, it poses a considerable threat to the health and comfort of residents.

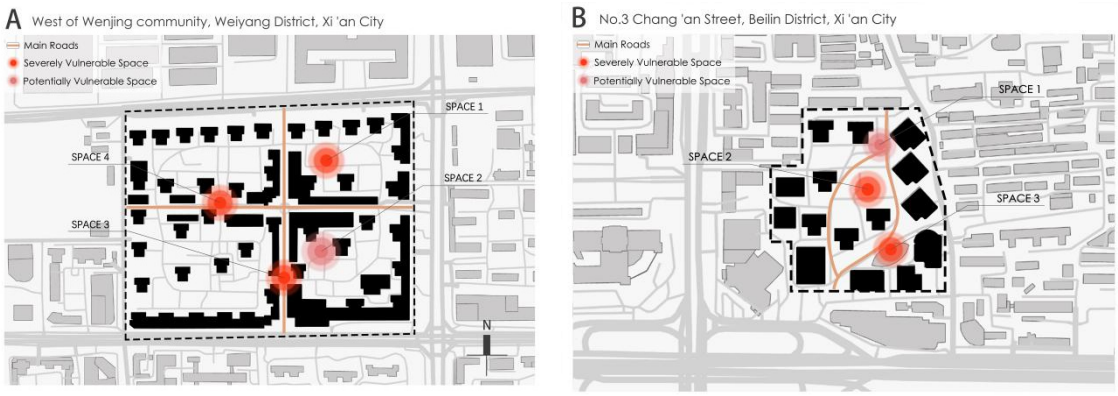

(**a**) (**b**)

Figure 14. Distribution of WHVSs in two cases. (**a**) Distribution of WHVSs in CASE A; (**b**) distribution of WHVSs in CASE B.

In the central part of the building complex within CASE A, there is a semi-enclosed space where wind speed remains below 0.5 m/s, and wind pressure is in a moderately negative state, as shown in Figure 14a. This phenomenon arises from the combined shielding effect of multiple buildings, which obstruct incoming airflow, causing it to converge and decelerate, thereby forming a low wind speed semi-enclosed zone. Given that this space is likely a primary activity area within the community with frequent human activity, particular attention should be paid to its ventilation performance and air quality to mitigate potential health risks.

In CASE A, areas with wind speeds ranging from 0.5 to 1.0 m/s are observed on the leeward sides of certain individual buildings, accompanied by slight negative pressure, as shown in Figure 14a. These zones primarily result from the wake effect generated by the buildings, leading to localized reductions in wind speed and the formation of slight negative pressure regions on the leeward side. Although the wind speed in these areas is relatively higher, facilitating stronger pollutant dispersion and limiting the environmental

impact to a smaller range, they exhibit good self-cleansing capacity and do not pose significant health risks.

2. CASE B: No. 3 Chang'an Street

On the southeast side of CASE B, there exists a large leeward zone where wind speed persistently remains below 0.5 m/s, as illustrated in Figure 14b. In this area, wind pressure is notably negative, ranging from approximately −0.5 to −1.5 Pa. The formation mechanism of this zone is attributed to the collective obstruction of incoming wind by the building complex, resulting in a large-scale separation zone on the leeward side. Here, airflow stagnates, creating poor ventilation conditions. The slow air movement in this region facilitates the accumulation of pollutants, significantly impacting the air quality and health of local residents.

The internal courtyard of CASE B also exhibits wind speeds below 0.5 m/s, with wind pressure stabilized between 0.5 and −1 Pa, as illustrated in Figure 14b. The high-rise buildings surrounding the courtyard create an enclosed space that restricts effective airflow and circulation, resulting in poor ventilation conditions within the courtyard. Given that the courtyard serves as a critical area for residents' daily activities, its inadequate ventilation poses significant risks to their health and comfort. Therefore, implementing effective measures to improve the courtyard's ventilation is essential.

For CASE B, localized wind speed zones ranging from 0.5 to 1.0 m/s were identified at specific building corners, accompanied by fluctuating negative pressure zones, as shown in Figure 14b. The formation of these areas is primarily attributed to airflow separation at the building corners, which generates localized vortices, resulting in wind speed fluctuations and negative pressure variations. Although the wind speeds in these zones are slightly higher than those in severely vulnerable areas, the vortex effect hinders the effective dispersion of pollutants. Therefore, the potential impact of these zones on air quality warrants attention.

Through the identification of WHVSs in two cases, both commonalities and differences in the distribution characteristics of vulnerable spaces are observed. In terms of commonality, the severely vulnerable areas at both locations are primarily concentrated in airflow dead zones and enclosed spaces formed between building clusters. These areas, due to low wind speeds and high negative pressures, become hotspots for pollutant accumulation. In terms of differences, the potential vulnerable areas in CASE A are mainly concentrated on the leeward sides of individual buildings, while the potential vulnerable areas in CASE B are distributed at building corners, forming localized vortices.

The identification results of WHVSs indicate that building layout and the blocking effect of high-rise buildings are the primary causes of wind environment vulnerability. In high-activity density areas, the deterioration of air quality due to crowd congregation has a more significant impact on residents' health. Therefore, for the identification of vulnerable spaces, not only should the physical characteristics of the wind environment be considered, but the spatial distribution and density of human activities must also be integrated to achieve a more accurate and comprehensive health risk assessment.

3.4. Validation of WHVS Identification

This section validates the identification of Wind Health-Vulnerable Spaces (WHVSs) by comparing the spatial distribution of simulated PM2.5 concentrations with field measurements in two representative high-rise residential areas (HRRAs). Despite differences in height settings and environmental conditions between the simulations and on-site monitoring, the consistency in spatial patterns supports the reliability of the model and the accuracy of WHVS identification.

3.4.1. Validation Method and Results

Based on the procedures detailed in Section 2.3, the validation involved comparing CFD-simulated PM2.5 distributions with multi-point monitoring data. The simulations utilized a standard k-ε turbulence model and an Eulerian dispersion model, with a maximum of 1.25 million mesh cells and a minimum grid size of 5 m. Boundary conditions were configured using typical winter meteorological data for Xi'an, including a prevailing wind direction of 270°, an average wind speed of 0.92 m/s, and a temperature range of 5–16 °C. Pollutant sources were defined as linear emissions from surrounding roads. To improve accuracy, an adaptive mesh refinement strategy was applied. The reliability of the CFD model was further validated through wind tunnel experiments using the AIJ standard model, yielding a root mean square error (RMSE) of 11.83%.

On-site PM2.5 measurements conducted on 21–22 December 2024 revealed peak concentrations of 89 μg/m^3 in CASE A and 77 μg/m^3 in CASE B. Figures 15 and 16 illustrate the spatial and temporal alignment between the simulated and measured concentrations at a pedestrian height of 1.5 m. In CASE A, pollutant hotspots in the northwest aligned with low wind speed zones, corresponding with peak measurements. In CASE B, the enclosed southeast courtyard exhibited persistent PM2.5 accumulation in both simulation and monitoring data, confirming the model's ability to identify critical low-ventilation areas.

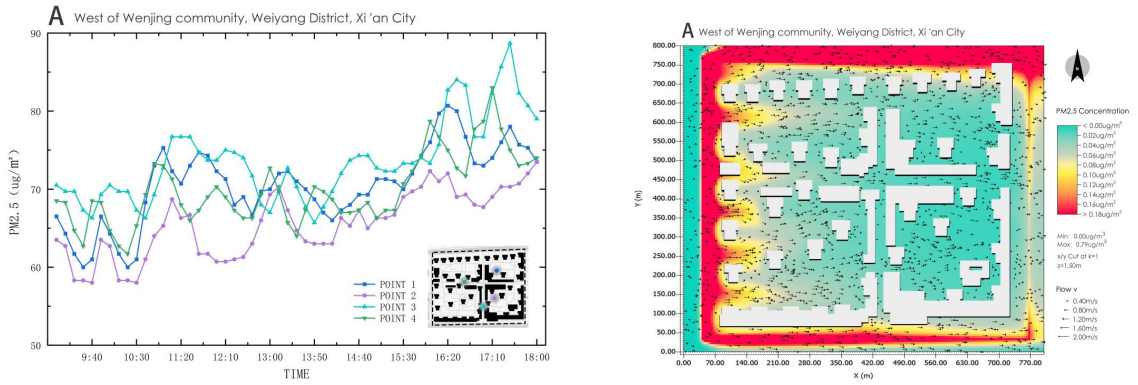

(**a**) (**b**)

Figure 15. Temporal variation curves of PM2.5 concentrations in CASE A. (**a**) Measured data; (**b**) simulated distribution.

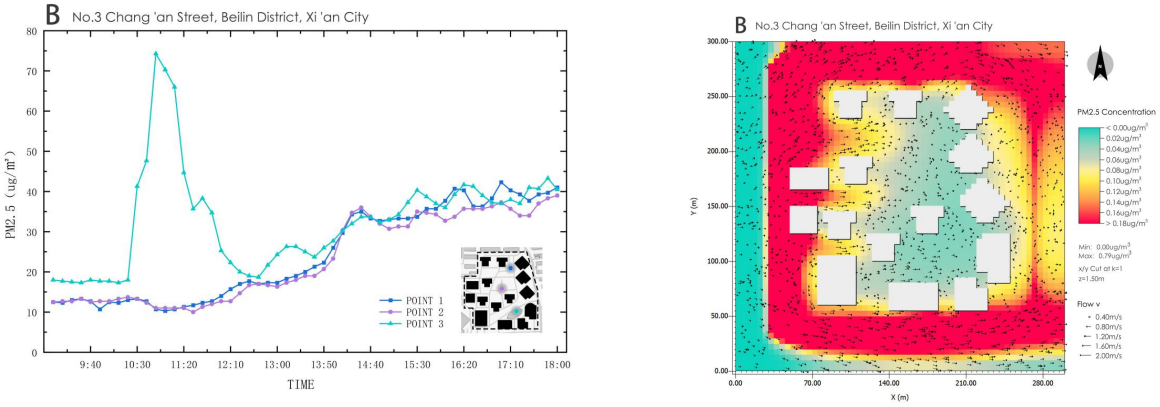

(**a**) (**b**)

Figure 16. Temporal variation curves of PM2.5 concentrations in CASE B. (**a**) Measured data; (**b**) simulated distribution.

Localized discrepancies were observed due to external environmental influences. First, regarding meteorological dynamics, the CFD simulations, which were based on steady-state conditions, did not account for instantaneous wind speed fluctuations. For example, in the southeastern portion of CASE B, a sudden increase in wind speed to 1.2 m/s at 11:00 on 22 December did not prevent elevated PM2.5 levels (measured: 78 $\mu g/m^3$; simulated: 62 $\mu g/m^3$). Second, in high-traffic zones such as the commercial core of CASE A, field measurements during the evening peak hours (18:00–20:00) exceeded simulated values by 15–20% due to human activity-related emissions (e.g., vehicles, respiration) that were not dynamically included in the CFD model.

3.4.2. Health Implications and Framework Outlook

The spatial coupling of PM2.5 concentrations with WHVSs further validated the effectiveness of health-vulnerable space identification. As shown in Figure 13, two typical WHVS types—localized calm zones between buildings (CASE A) and large-scale weak wind areas in enclosed layouts (CASE B)—exhibited strong spatial overlap with PM2.5 hotspots. Additionally, the spatial superposition of POI activity hotspots (e.g., the internal courtyard of CASE B, Figure 13) and low wind speed zones amplified health exposure risks (Figure 14b). These findings support the dual mechanism of WHVS formation: wind field disturbances induced by building morphology and spatial aggregation effects of human activities. Notably, previous studies have linked PM2.5 exposure to elevated health risks. Liu et al. found that every 10 $\mu g/m^3$ increase in PM2.5 concentration was associated with a 0.55% increase in cardiovascular mortality across 652 cities worldwide [10]. This reinforces the health relevance of identifying WHVS in high-density residential environments.

The validation results confirm that the multidimensional CFD-POI-monitoring framework provides a robust approach for identifying WHVSs in high-rise residential areas, with simulated PM2.5 distributions closely matching measured data in critical low-ventilation zones. To further assess the potential influence of simulation errors on WHVS identification outcomes, this study analyzed the 11.83% mean error between the CFD simulations and wind tunnel experiments. Blocken et al. [4] and Tominaga et al. [34] demonstrated that a CFD simulation error of 10–15% is generally acceptable for wind environment simulations in complex urban settings, and the 11.83% mean error observed in this study falls within this acceptable range. Furthermore, Toparlar et al. [32] noted that when the research objective is to identify regional wind environment characteristics rather than to predict precise wind speed values, an error within 15% does not significantly impact the study's conclusions. In addition, the simulated PM2.5 concentration distribution exhibited a high degree of spatial consistency with field measurements in critical low-ventilation areas, further validating the reliability and effectiveness of the WHVS identification method proposed in this study.

To further enhance the applicability of this framework, future research could explore the integration of real-time meteorological dynamics (e.g., coupling with mesoscale weather models) and refine emission source characterization through more granular traffic or activity-level data. Moreover, extending the analysis to multi-pollutant interactions (e.g., NO_x and bioaerosols) would deepen the understanding of cumulative health risks. These advancements will strengthen the framework's adaptability to diverse urban contexts while maintaining its foundational value in guiding health-centric architectural and environmental design practices.

3.4.3. Graphical Comparison of WHVS-Related Indicators

To further enhance the interpretability of the results, four key environmental risk indicators were visualized to compare CASE A and CASE B: (1) the proportion of low wind speed zones ($v < 0.5$ m/s), (2) the proportion of negative wind pressure zones ($p < 0$ Pa),

(3) the proportion of high-density human activity areas (Levels 6–7), and (4) the maximum PM2.5 concentration measured on-site.

As illustrated in Figure 17, CASE B exhibits higher proportions of low wind speed (48%) and negative pressure zones (41%), indicating a more obstructed wind environment. CASE A, in contrast, shows slightly higher human activity concentration (19%) and pollutant accumulation (89 μg/m^3). This visual comparison quantitatively supports the classification of WHVSs by highlighting the spatial co-occurrence of poor wind performance and health-related exposure risks.

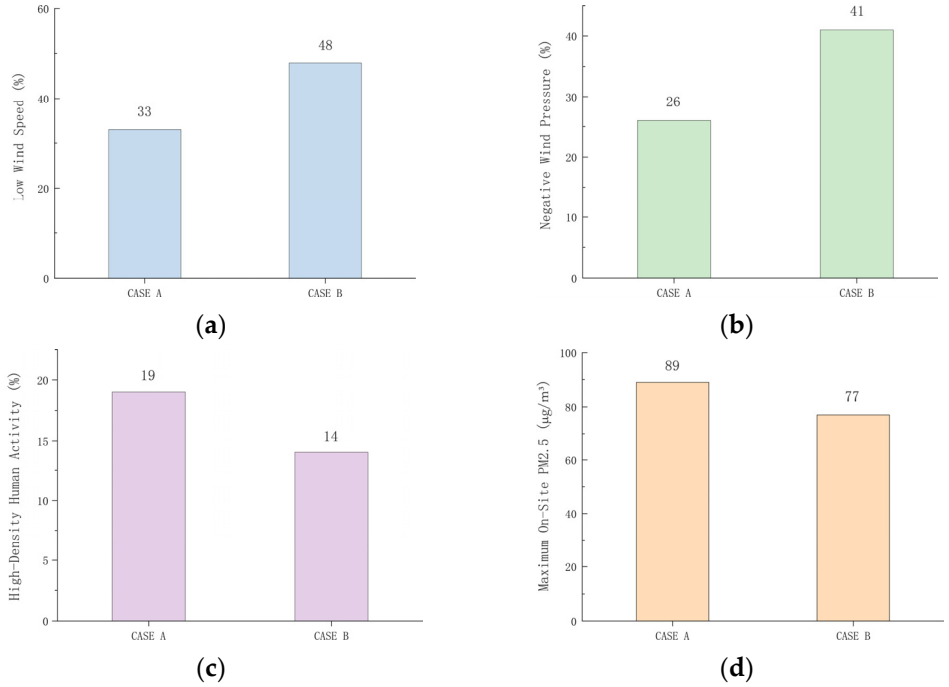

Figure 17. Comparative analysis of four WHVS-related environmental indicators between CASE A and CASE B. (**a**) Low wind speed area ratio (v < 0.5 m/s); (**b**) negative wind pressure area ratio (p < 0 Pa); (**c**) high-density human activity ratio (Levels 6–7); (**d**) maximum on-site PM2.5 concentration (μg/m^3).

4. Discussion

4.1. Main Research Findings

This study identified and diagnosed the WHVSs of two typical HRRAs in Xi'an through a combination of CFD simulations, POI data analysis, and field monitoring. The following main findings were obtained:

1. Wind Environment Distribution Patterns

The study revealed significant spatial variations in pedestrian-level wind environments (1.5 m height). In CASE A, building clusters caused airflow interference, forming a continuous low wind speed zone (<0.5 m/s) on the northwest side with stable negative pressure (−0.5 to 3 Pa). In CASE B, a large leeward area on the southeast side exhibited consistently low wind speeds (<0.5 m/s) and stronger negative pressure (−1 to −2 Pa).

The distribution patterns are governed by three factors:

① Building Layout and Density: Dense arrangements amplify airflow obstruction;

② Building Spacing and Height: Narrow gaps and tall structures intensify turbulence;

③ Enclosure Effects: Enclosed courtyards trap pollutants.

Table 2 summarizes the comparative analysis of wind environment characteristics and their impact mechanisms, validated by field measurements.

Table 2. Comparison of wind environment characteristics and impact mechanisms in CASE A and CASE B.

Characteristics	CASE A	CASE B
Location of Low Wind Speed Areas	Gaps between buildings on the northwest side	Leeward areas of buildings on the southeast side and internal courtyards
Extent of Low Wind Speed Areas	Localized regions	Large-scale areas
Wind Speed Feature	<0.5 m/s	<0.5 m/s
Characteristics of Wind Pressure	−0.5 to 3 Pa (the negative pressure zone is concentrated in the shaded regions of the buildings)	−1 to −2 Pa (the negative pressure zone is concentrated in the leeward areas)
Formation Mechanism	The dense arrangement of buildings causes airflow separation and vortex formation	The closed arrangement of buildings results in wind shadow effects and recirculation patterns
Main Effect	Low ventilation efficiency leads to the accumulation of pollutants	Poor ventilation conditions result in the accumulation of pollutants within the courtyard
Extent of Low Wind Speed Areas	Localized regions	Large-scale areas

2. Vulnerable Space Characteristics

The WHVSs exhibit distinct locational characteristics. The severely vulnerable areas identified in the study are mainly located in the airflow dead zones and enclosed spaces formed by the building clusters. These areas are typically characterized by low wind speeds (<0.5 m/s) and negative pressure, which hinder pollutant dispersion. More importantly, these areas significantly overlap with high-frequency human activity spaces, such as main pedestrian pathways and public activity areas, exacerbating potential health risks. The study identified two typical forms of wind environment health-vulnerable spaces: first, localized calm wind zones formed between buildings, such as the low-speed region between building clusters on the northwest side of CASE A's western area; second, large-scale weak wind areas formed by building enclosures, such as the internal courtyard space of CASE B.

3. Formation Mechanism

Through comprehensive analysis, this study revealed a dual mechanism behind the formation of wind environment health-vulnerable spaces.

First, wind field disturbances caused by the building layout: the blocking effect of high-rise building clusters and their spacing directly affect the airflow organization at pedestrian height.

Second, the superimposed effect of human activity distribution: POI data analysis shows that human activities are often concentrated in public spaces formed by building enclosures, and the overlap of this spatial usage pattern with unfavorable wind environments exacerbates exposure risks.

Taking the western area of CASE B as an example, the layout of the central building clusters not only created a stable calm wind zone but also, as it was the main human activity area, significantly increased exposure risks. This indicates that the formation of vulnerable spaces is a result of the combined effects of the physical environment of buildings and human behavior, offering a new perspective for health-oriented residential planning.

Moreover, geometric parameters such as the building height-to-width ratio (H/W) and spacing have been shown to exert measurable influences on wind field characteristics. For instance, Oke noted that when H/W exceeds 0.65, skimming flow dominates, significantly suppressing vertical ventilation [38]. Zhang et al. conducted field measurements and simulations in Xi'an, demonstrating that increased building spacing enhances wind speed distribution and ventilation efficiency within residential complexes [39]. These findings

provide theoretical and empirical support for understanding how geometric configurations of dense layouts contribute to the formation of WHVSs.

4.2. Innovation and Contribution

Theoretical Innovation: This study proposes the concept of WHVSs, extending the theory of spatial vulnerability from the macro-scale of urban areas to the micro-scale of building environments. This enriches the application of the related theory across different spatial scales. Furthermore, by integrating three dimensions—WEC, pollutant distribution, and crowd activities—this study constructs a more comprehensive evaluation framework.

Methodological Innovation: A multidimensional analysis framework based on CFD-POI monitoring was developed. By using CFD simulations to obtain refined WEC, analyzing crowd activity patterns with POI data, and validating the results with PM2.5 monitoring, this study achieves a quantitative coupling analysis of wind environment and crowd activities. This method provides a new technological approach for evaluating the wind environment health of HRRAs.

Practical Guidance Value: The findings of this study provide a theoretical basis and practical guidance for improving wind environment quality in HRRAs and safeguarding the health of residents. By identifying the distribution characteristics and formation mechanisms of vulnerable spaces, this research offers specific references for residential planning, design, and environmental optimization.

4.3. Limitations

Temporal and Seasonal Considerations: This study focuses on winter conditions in Xi'an and includes two representative high-rise residential types. The findings may not fully capture layout variations across other climates or urban settings. Future research should extend to other seasons and common typologies, such as tower–podium forms, to improve generalizability.

Methodological Approach: The steady-state CFD simulations effectively identify persistent wind patterns but cannot capture transient meteorological phenomena. This approach, while aligned with research objectives, has inherent constraints in representing dynamic ventilation effects and flow separation around building edges.

Parametric Specificity: The analysis attributes wind environment characteristics to broad layout typologies rather than systematically quantifying how specific building parameters independently influence wind fields. A more parametric approach in future studies could facilitate the development of precise design guidelines based on quantitative thresholds.

Data Granularity: The POI data successfully captured spatial activity patterns, though more refined individual exposure metrics would require supplementary datasets. Future research could integrate GPS tracking data to provide more comprehensive information regarding exposure duration and frequency within urban environments.

Temporal Robustness: The field monitoring in this study was limited to a short period during the winter season. While this timeframe reflects typical peak pollution conditions, its temporal limitation may overlook seasonal variations and transient meteorological influences, thereby affecting the robustness of the conclusions. Future research should incorporate multi-seasonal data to enhance the temporal generalizability of the findings.

Translational Framework: While establishing significant correlations between wind environments and PM2.5 concentrations, this study does not extend to quantitative health impact metrics. Integration with epidemiological datasets and population-specific concentration–response functions represents an opportunity for subsequent research to enhance practical applications.

5. Conclusions

This study proposed the concept of Wind Health-Vulnerable Spaces (WHVSs) and developed a multidimensional framework for their identification in high-rise residential areas by integrating CFD simulations, POI data, and field monitoring. Two types of WHVSs were identified. In CASE A, localized calm zones (wind speed < 0.5 m/s, pressure −0.5 to 3 Pa) were found between densely arranged buildings, where PM2.5 concentrations reached up to 89 $\mu g/m^3$. In CASE B, large-scale weak wind areas (wind speed < 0.5 m/s, pressure −1 to −2 Pa) were observed in enclosed layouts, with monitored PM2.5 levels rising to 77 $\mu g/m^3$—significantly higher than the surrounding well-ventilated zones.

The formation of these WHVSs can be attributed to a dual mechanism: wind field disruptions caused by building morphology and the spatial overlap of these zones with high-frequency human activity areas such as intersections and courtyards. CFD simulations effectively captured the spatial distribution of pollutant accumulation, showing strong agreement with field measurements.

These findings provide both methodological and empirical support for integrating health risk diagnosis into residential planning and highlight the importance of coupling physical wind environment assessments with human behavioral patterns in future urban design.

Building on this foundation, future research should enhance the framework's temporal robustness by incorporating multi-seasonal monitoring and transient CFD simulations to capture short-term wind variability. Applying the WHVS approach to diverse residential typologies, such as tower–podium forms, would improve its generalizability. Parametric studies on specific building attributes—such as height, spacing, and orientation—may support the development of quantitative ventilation guidelines. Integrating individual-level mobility data, such as GPS-based tracking, can enable more refined exposure assessments. Finally, linking environmental indicators with epidemiological datasets through concentration–response models would advance the framework's potential for health-oriented urban design.

Supplementary Materials: POI data can be downloaded at: https://lbs.amap.com (accessed on 30 November 2024).

Author Contributions: J.C. and S.M. contributed equally to this work. Conceptualization, J.C., S.M. and J.R.; methodology, S.M., J.C. and J.R.; software, S.M. and J.C.; validation, J.C. and S.M.; formal analysis, J.C. and S.M.; investigation, S.M., J.C. and Y.M.; resources, S.M., J.C., Y.M. and J.R.; data curation, S.M., J.C. and Y.M.; writing—original draft preparation, J.C., S.M., Y.M. and J.R.; writing—review and editing, J.C., S.M., Y.M., Y.L. and J.R.; visualization, J.C., S.M. and Y.M.; supervision, Y.L. and J.R.; project administration, J.R.; funding acquisition, J.R. All authors have read and agreed to the published version of the manuscript.

Funding: National Key Research and Development Program of China, grant number: 2023YFB3002800; Department of Science and Technology of Shaanxi Province, grant number: 2024GH-ZDXM-03.

Data Availability Statement: The data presented in this study are available on request from the corresponding author.

Conflicts of Interest: The authors declare no conflicts of interest.

Appendix A

Table A1. Advances in research on the health impacts of outdoor wind environments in residential areas (2006–2025).

Researchers (Year)	Research Scale	Key Findings	Methodology
Bai et al. (2006) [20]	Urban Residential Clusters	Revealed densification and functional change in Xi'an's residential space from 2006 to 2022, driven by policy and market forces.	GIS and temporal analysis of housing data.
Kubota et al. (2008) [6]	Residential Neighborhoods	Identified correlations between building density and pedestrian wind speed; proposed design guidelines for comfortable wind environments.	Wind tunnel experiments on varied density scenarios.
Brook et al. (2010) [8]	Human Health	Confirmed strong associations between PM exposure and cardiovascular diseases; emphasized both short- and long-term risks.	Scientific statement based on epidemiological and clinical evidence review.
Tominaga et al. (2011) [12]	Street Canyon	Compared LES and RANS for street canyon pollutant dispersion; found LES provides better detail but at higher computational cost.	CFD simulations comparing LES and RANS models.
Ramponi et al. (2012) [15]	Single Isolated Building	Evaluated how different CFD parameters such as turbulence models and mesh resolution influence cross-ventilation accuracy. Emphasized the importance of parameter selection in reliable simulation.	Parametric CFD simulations on a simplified building.
Zhao et al. (2013) [19]	National (China-wide)	Tracked national trends of PM2.5 and ozone pollution from 2013 to 2020 and quantified the associated health burden. Highlighted spatial differences and the effectiveness of policy measures.	Multi-source emission data analysis and health impact modeling.
Ai et al. (2013) [7]	Single Building	Investigated how inhomogeneous atmospheric boundary layers and near-wall treatments affect flow and pollutant dispersion. Demonstrated that ABL profiles significantly influence simulation accuracy.	CFD simulations with varied ABL and wall treatments.
Aflaki et al. (2015) [16]	Building-Scale	Reviewed natural ventilation strategies using façade elements in tropical climates. Highlighted key design factors affecting ventilation performance.	Systematic literature review on natural ventilation design.

Table A1. *Cont.*

Researchers (Year)	Research Scale	Key Findings	Methodology
Kim et al. (2015) [9]	Human Health	Summarized epidemiological evidence linking particulate matter exposure to cardiovascular, respiratory, and neurological diseases; emphasized the vulnerability of children and the elderly.	Comprehensive review of clinical and population-based studies on PM health effects.
Li et al. (2015) [13]	Building Passageways	Reassessed the Venturi effect in passage ventilation between non-parallel buildings; showed that shape and angle strongly influence airflow acceleration and ventilation efficiency.	CFD simulations analyzing geometric configurations and flow behavior.
Blocken et al. (2016) [4]	Pedestrian-Level (Building Surroundings)	Reviewed wind tunnel and CFD approaches for assessing pedestrian wind comfort; compared accuracy, limitations, and recommended best practices for reliable evaluations.	Comparative review of experimental and numerical methods in wind comfort research.
Tong et al. (2016) [3]	Naturally Ventilated Building	Quantified how outdoor traffic-related air pollution infiltrates indoor spaces through natural ventilation; revealed significant indoor exposure to PM and black carbon.	Field measurements and statistical analysis of pollutant infiltration patterns.
Mittal et al. (2018) [5]	Pedestrian-Level (Urban Buildings)	Reviewed key parameters influencing pedestrian-level wind around buildings, including layout, height, and orientation; emphasized simulation and experimental techniques.	Literature review of CFD, wind tunnel, and empirical studies.
Ai et al. (2018) [14]	Building Adjacent to Street Canyon	Analyzed how street canyon geometry and façade design affect wind-driven single-sided ventilation; identified configurations that enhance indoor airflow.	CFD simulations assessing various street layouts and envelope designs.
Liu et al. (2019) [10]	Global (652 Cities)	Found a significant association between short-term PM2.5 exposure and increased daily mortality across diverse climatic and economic contexts.	Multi-country time-series analysis using standardized epidemiological models.
Ma et al. (2019) [2]	National (China)	Analyzed spatial coupling between regional economic growth and urbanization; revealed strong spatial heterogeneity and identified leading industrial sectors in coordinated regions.	Spatial statistical analysis using coupling coordination models and industrial structure evaluation.

Table A1. *Cont.*

Researchers (Year)	Research Scale	Key Findings	Methodology
United et al. (2020) [1]	Global Urban Trends	Projected that by 2050, 68% of the global population will live in cities, with the fastest growth in Asia; emphasized sustainable urbanization as key to equitable development.	Global urban data synthesis and policy-oriented analysis.
Huang et al. (2021) [11]	High-Rise Urban Area	Demonstrated that high-rise buildings significantly alter wind fields and pollutant dispersion, with effects varying under different atmospheric temperature stratifications.	CFD simulations under multiple thermal stratification scenarios.
Chen et al. (2023) [17]	Building Form Effects	Podium-connected towers reduced dispersion efficiency in winter.	3D CFD under thermal stratification.
Li et al. (2024) [18]	Multi-city Risk Assessment	Developed and validated a Wind Health Risk Index.	Integrated CFD–GIS modeling with health risk assessment.
Huo et al. (2025) [21]	Urban Residential Clusters	Analyzed long-term urban structure changes in Xi'an from 2000 to 2020; revealed that increasing building density and spatial infill significantly elevated urban heat stress levels in high-density residential areas.	Remote sensing-based urban form tracking and spatial correlation analysis between morphological metrics and heat stress indicators.

Note: CFD = computational fluid dynamics; PM2.5 = particulate matter 2.5; LES = Large Eddy Simulation; RANS = Reynolds-Averaged Navier–Stokes.

References

1. United Nations Human Settlements Programme. *World Cities Report 2020: The Value of Sustainable Urbanization*; UN-Habitat: Nairobi, Kenya, 2020. Available online: https://unhabitat.org/world-cities-report-2020-the-value-of-sustainable-urbanization (accessed on 16 April 2025).
2. Ma, L.; Jin, F. Spatial Pattern and Industrial Sector Structure Analysis on the Coupling and Coordinating Degree of Regional Economic Development and Environmental Pollution in China. *Acta Geogr. Sin.* **2012**, *67*, 1299–1307.
3. Tong, Z.; Chen, Y.; Malkawi, A.; Adamkiewicz, G.; Spengler, J. Quantifying the impact of traffic-related air pollution on the indoor air quality of a naturally ventilated building. *Environ. Int.* **2016**, *89*, 138–146. [CrossRef] [PubMed]
4. Blocken, B.; Stathopoulos, T.; van Beeck, J. Pedestrian-level wind conditions around buildings: Review of wind-tunnel and CFD techniques and their accuracy for wind comfort assessment. *Build. Environ.* **2016**, *100*, 50–81. [CrossRef]
5. Mittal, H.; Sharma, A.; Gairola, A. A review on the study of urban wind at the pedestrian level around buildings. *J. Build. Eng.* **2018**, *18*, 154–163. [CrossRef]
6. Kubota, T.; Miura, M.; Tominaga, Y.; Mochida, A. Wind tunnel tests on the relationship between building density and pedestrian-level wind velocity: Development of guidelines for realizing acceptable wind environment in residential neighborhoods. *Build. Environ.* **2008**, *43*, 1699–1708. [CrossRef]
7. Ai, Z.T.; Mak, C.M. CFD Simulation of Flow and Dispersion around an Isolated Building: Effect of Inhomogeneous ABL and Near-Wall Treatment. *Atmos. Environ.* **2013**, *77*, 568–578. [CrossRef]
8. Brook, R.D.; Rajagopalan, S.; Pope, C.A., III; Brook, J.R.; Bhatnagar, A.; Diez-Roux, A.V.; Holguin, F.; Hong, Y.; Luepker, R.V.; Mittleman, M.A.; et al. Particulate matter air pollution and cardiovascular disease: An update to the scientific statement from the American Heart Association. *Circulation* **2010**, *121*, 2331–2378. [CrossRef] [PubMed]
9. Kim, K.-H.; Kabir, E.; Kabir, S. A review on the human health impact of airborne particulate matter. *Environ. Int.* **2015**, *74*, 136–143. [CrossRef]
10. Liu, C.; Chen, R.; Sera, F.; Vicedo-Cabrera, A.M.; Guo, Y.; Tong, S.; Coelho, M.S.Z.S.; Saldiva, P.H.N.; Lavigne, E.; Matus, P.; et al. Ambient particulate air pollution and daily mortality in 652 cities. *N. Engl. J. Med.* **2019**, *381*, 705–715. [CrossRef]

11. Huang, X.; Gao, L.; Gu, D.; Yao, R. Impacts of High-Rise Building on Urban Airflows and Pollutant Dispersion under Different Temperature Stratifications: Numerical Investigations. *Atmos. Pollut. Res.* **2021**, *12*, 138–146. [CrossRef]
12. Tominaga, Y.; Stathopoulos, T. CFD Modeling of Pollution Dispersion in a Street Canyon: Comparison between LES and RANS. *J. Wind Eng. Ind. Aerodyn.* **2011**, *99*, 340–348. [CrossRef]
13. Li, B.; Luo, Z.; Sandberg, M.; Liu, J. Revisiting the 'Venturi Effect' in Passage Ventilation between Two Non-Parallel Buildings. *Build. Environ.* **2015**, *94*, 714–722. [CrossRef]
14. Ai, Z.T.; Mak, C.M. Wind-Induced Single-Sided Natural Ventilation in Buildings Near a Long Street Canyon: CFD Evaluation of Street Configuration and Envelope Design. *J. Wind Eng. Ind. Aerodyn.* **2018**, *172*, 96–106. [CrossRef]
15. Ramponi, R.; Blocken, B. CFD Simulation of Cross-Ventilation for a Generic Isolated Building: Impact of Computational Parameters. *Build. Environ.* **2012**, *53*, 34–48. [CrossRef]
16. Aflaki, A.; Mahyuddin, N.; Al-Cheikh Mahmoud, Z.; Baharum, M.R. A Review on Natural Ventilation Applications through Building Façade Components and Ventilation Openings in Tropical Climates. *Energy Build.* **2015**, *101*, 153–162. [CrossRef]
17. Chen, Y.; Pathirana, A.; De Silva, C.S.; Bandara, C. Air Pollutant Dispersion around High-Rise Building Cluster Forms: The Case of Port City Colombo, Sri Lanka. *Build. Environ.* **2023**, *237*, 110315. [CrossRef]
18. Back, Y.; Kumar, P.; Bach, P.M.; Rauch, W.; Kleidorfer, M. Integrating CFD-GIS Modelling to Refine Urban Heat and Thermal Comfort Assessment. *Sci. Total Environ.* **2023**, *858 Pt 1*, 159729. [CrossRef]
19. Xiao, Q.; Geng, G.; Xue, T.; Liu, S.; Cai, C.; He, K.; Zhang, Q. Tracking PM2.5 and O3 Pollution and the Related Health Burden in China from 2013 to 2020. *Environ. Sci. Technol.* **2021**, *56*, 6922–6932. [CrossRef]
20. Bai, X.; Wu, W.; Liu, L.; Shang, W.; Dong, H. Spatio-Temporal Evolution and Implications of Urban Residential Space Based on the New Commercial Housing in Xi'an, China, 2006–2022. *Sustainability* **2024**, *16*, 8495. [CrossRef]
21. Huo, K.; Qin, R.; Zhao, J.; Wang, Y.; Liu, M. Long-Term Tracking of Urban Structure and Analysis of Its Impact on Urban Heat Stress: A Case Study of Xi'an, China. *Ecol. Indic.* **2025**, *174*, 113418. Available online: https://www.sciencedirect.com/science/article/pii/S1470160X25003486 (accessed on 16 April 2025). [CrossRef]
22. Yuan, C.; Ng, E.; Norford, L.K. Improving Air Quality in High-Density Cities by Understanding the Relationship between Air Pollutant Dispersion and Urban Morphologies. *Build. Environ.* **2014**, *71*, 245–258. [CrossRef]
23. Lateb, M.; Meroney, R.N.; Yataghene, M.; Fellouah, H.; Saleh, F.; Boufadel, M.C. On the Use of Numerical Modelling for Near-Field Pollutant Dispersion in Urban Environments—A Review. *Environ. Pollut.* **2016**, *208*, 271–283. [CrossRef]
24. Yang, J.; Shi, B.; Zheng, Y.; Shi, Y.; Xia, G. Urban Form and Air Pollution Disperse: Key Indexes and Mitigation Strategies. *Sustain. Cities Soc.* **2020**, *57*, 101955. [CrossRef]
25. Jin, Y.; Andersson, H.; Zhang, S. Air Pollution Control Policies in China: A Retrospective and Prospects. *Int. J. Environ. Res. Public Health* **2016**, *13*, 1219. [CrossRef]
26. Jiao, W.; Hagler, G.; Williams, R.; Sharpe, R.; Brown, R.; Garver, D.; Judge, R.; Caudill, M.; Rickard, J.; Davis, M.; et al. Community Air Sensor Network (CAIRSENSE) Project: Evaluation of Low-Cost Sensor Performance in a Suburban Environment in the Southeastern United States. *Atmos. Meas. Tech.* **2016**, *9*, 5281–5292. [CrossRef]
27. Blocken, B. Computational Fluid Dynamics for Urban Physics: Importance, Scales, Possibilities, Limitations and Ten Tips and Tricks towards Accurate and Reliable Simulations. *Build. Environ.* **2015**, *91*, 219–245. [CrossRef]
28. Di Sabatino, S.; Buccolieri, R.; Pulvirenti, B.; Britter, R. Simulations of Pollutant Dispersion within Idealised Urban-Type Geometries with CFD and Integral Models. *Atmos. Environ.* **2007**, *41*, 8316–8329. [CrossRef]
29. Ng, E.; Yuan, C.; Chen, L.; Ren, C.; Fung, J.C.H. Improving the Wind Environment in High-Density Cities by Understanding Urban Morphology and Surface Roughness: A Study in Hong Kong. *Landsc. Urban Plan.* **2011**, *101*, 59–74. [CrossRef]
30. Turner, B.L.; Kasperson, R.E.; Matson, P.A.; McCarthy, J.J.; Corell, R.W.; Christensen, L.; Eckley, N.; Kasperson, J.X.; Luers, A.; Martello, M.L.; et al. A Framework for Vulnerability Analysis in Sustainability Science. *Proc. Natl. Acad. Sci. USA* **2003**, *100*, 8074–8079. [CrossRef]
31. Jiang, G.; Wu, M.; Hu, T. Turbulence and Pollutant Statistics around a High-Rise Building with and without Overhangs. *Atmosphere* **2023**, *14*, 1771. [CrossRef]
32. Toparlar, Y.; Blocken, B.; Maiheu, B.; van Heijst, G.J.F. A review on the CFD analysis of urban microclimate. *Renew. Sustain. Energy Rev.* **2017**, *80*, 1613–1640. [CrossRef]
33. Zheng, C.; Li, Y.; Wu, Y. Pedestrian-level wind environment on outdoor platforms of a thousand-meter-scale megatall building: Sub-configuration studies of wind comfort based on thermal environment considerations. *Build. Environ.* **2016**, *106*, 82–101. [CrossRef]
34. Tominaga, Y.; Mochida, A.; Yoshie, R.; Kataoka, H.; Nozu, T.; Yoshikawa, M.; Shirasawa, T. AIJ guidelines for practical applications of CFD to pedestrian wind environment around buildings. *J. Wind Eng. Ind. Aerodyn.* **2008**, *96*, 1749–1761. [CrossRef]
35. Tsang, C.W.; Kwok, K.C.S.; Hitchcock, P.A. Wind tunnel study of pedestrian level wind environment around tall buildings: Effects of building dimensions, separation and podium. *Build. Environ.* **2012**, *49*, 167–181. [CrossRef]

36. Liu, Q.; Zhang, Y.; Ma, W.; Ren, J. Application of an architect-friendly digital design approach to the wind environment of campus dormitory buildings. *Sustainability* **2023**, *15*, 9168. [CrossRef]
37. Chen, Z.; Wang, J.; Ma, G.; Zhang, Y. Understanding Meteorological Influences on PM2.5 Concentrations across China: A Temporal and Spatial Perspective. *Atmos. Chem. Phys.* **2018**, *18*, 5343–5358. [CrossRef]
38. Oke, T.R. Street Design and Urban Canopy Layer Climate. *Energy Build.* **1988**, *11*, 103–113. [CrossRef]
39. Zhang, Q.; Zhou, D.; Xu, D.; Rogora, A. Association between Wind Environment and Spatial Characteristics of High-Rise Residential Buildings in Cold Regions through Field Measurements in Xi'an. *Buildings* **2023**, *13*, 2007. [CrossRef]